Photophysics and Photochemistry of the UV Filter Kynurenine Covalently Attached to Amino Acids and to a Model Protein

Peter S. Sherin,*,†,‡ Jakob Grilj,‡ Lyudmila V. Kopylova,† Vadim V. Yanshole,† Yuri P. Tsentalovich,† and Eric Vauthey‡

International Tomography Center SB RAS, Institutskaya str. 3a, 630090 Novosibirsk, Russia, and Department of Physical Chemistry, University of Geneva, quai Ernest-Ansermet 30, CH-1211 Geneva, Switzerland

Received: May 17, 2010; Revised Manuscript Received: August 3, 2010

The photophysics and photochemistry of kynurenine (KN) covalently bound to the amino acids lysine, cysteine, and histidine, the antioxidant glutathione, and the protein lysozyme have been studied by optical spectroscopy with femto- and nanosecond time resolution. The fluorescence quantum yield of the adducts of KN to amino acids is approximately 2 times higher than that of the free KN in solution; KN attached to protein exhibits a 7-fold increase in the fluorescence quantum yield. The S_1 state dynamics of KN-modified lysozyme reveals a multiphasic decay with a broad dispersion of time constants from 1 ps to 2 ns. An increase of the triplet yield of KN bound to lysozyme is also observed; the triplet state undergoes fast intramolecular decay. The obtained results reveal an increase of the photochemical activity of KN after its covalent attachment to amino acids and proteins, which may contribute to the development of oxidative stress in the human lenses—the main causative factor for the cataract onset.

Introduction

Our eyes are protected from UV irradiation by low-molecular-weight molecules contained in the lens, kynurenine (KN) and its derivatives.[1−4] These natural metabolites of the amino acid tryptophan absorb UV light in the 300−400 nm region and exhibit low photochemical activity,[5−8] which allows the function of kynurenines as UV filtering molecules, protecting the eye tissues from the harmful UV irradiation. The most abundant UV filters in the lens are (in decreasing order): 3-hydroxykynurenine *O*-β-D-glucoside (3OHKG), 4-(2-amino-3-hydroxyphenyl)-4-oxobutanoic acid *O*-β-D-glucoside (AHBG), kynurenine (KN), and 3-hydroxykynurenine (3OHKN).

Kynurenine-based UV filters (3OHKG, KN, and 3OHKN) are thermally unstable molecules under physiological conditions:[9,10] the spontaneous fragmentation (deamination) leads to the formation of α,β-unsaturated compounds—carboxyketoalkenes (CKAs)[10−12]—which can covalently bind to nucleophilic residues of the lens proteins—cysteine (Cys), histidine (His), and lysine (Lys).[10,13−16] A covalent attachment of the UV filters to the lens proteins has been shown to be one of the numerous age-related post-translational modifications of the lens proteins.[9,11,13] CKAs can also react with the reduced gluthatione (GSH), forming the GSH-KN, GSH-3OHKN, and GSH-3OHKG adducts.[10,14,17] With aging, the concentration of free UV filters in the lens decreases, whereas the levels of GSH-bound and protein-bound kynurenines increase.[18] These processes can increase the susceptibility of the lens tissue to UV irradiation: the KN adducts absorb in the UV-A wavelength region as well as the free UV filters, but they are photochemically more active than the parent compound KN: in a neutral aqueous solution, the adducts are more fluorescent[15,19] and exhibit higher triplet yields.[20] The generation of reactive oxygen species (ROS) upon aerobic photolysis of lens proteins modified by KN and its derivatives has been reported.[21,22] The underlying mechanism, however, remains unclear. Thus, the photochemical reactions of KN-modified lens proteins may accelerate the aging processes and give a contribution to the cataract development.

Recently, we reported a detailed study of the photophysics of KN.[23] It has been revealed that the lifetime of the singlet excited state S_1 (τ_s) is highly sensitive to the nature of the local environment: in aqueous solutions, τ_s is about 30 ps, it increases in alcohols by an order of magnitude, and it exceeds 1 ns in the aprotic solvents dimethylformamide (DMF) and dimethyl sulfoxide (DMSO). The change of the medium character from protic to aprotic also leads to a tremendous increase of the triplet quantum yield (from 1.7% in aqueous solution to 35% in DMSO).[23] It has been shown that solvent-assisted internal conversion (IC) is the main deactivation channel of the S_1 state in protic solvents: the rate constant of the fast radiationless $S_1 \rightarrow S_0$ transition is determined by the ability of the solvent to form hydrogen bonds with KN. This may explain the increased photoactivity of protein-bound UV filters in comparison to the free ones: in the hydrophobic environment of a protein, the IC rate constant decreases, so the lifetime of the singlet excited state and the yield of the chemically active triplet state increase. The latter can be readily quenched by oxygen, by the antioxidant ascorbate, and by the amino acids tryptophan and tyrosine.[24] The peroxides and the products of tyrosine oxidation, observed after UV irradiation of UV filter-modified lens proteins,[21,22] may originate from the reactions of triplet UV filters with molecular oxygen and tyrosine residues of lens proteins.

At present, there is no report on the photophysics and photochemistry of the lens proteins modified by UV filters and the present work is a first step toward this. The main goal of this work is to examine the photochemical activity of KN covalently bound to biologically relevant molecules: (a) to the amino acids cysteine (Cys-KN), histidine (His-KN), and lysine (Lys-KN), (b) to the antioxidant glutathione (GSH-KN), which is present in the human lens,[18] and (c) to a protein molecule.

* Corresponding author. Phone: +7-383-330-31-36. Fax: +7-383-333-13-99. E-mail: Sherin@tomo.nsc.ru, Petr.Sherin@unige.ch.
† International Tomography Center SB RAS.
‡ University of Geneva.

10.1021/jp104485k
Published on Web 08/19/2010

CHART 1

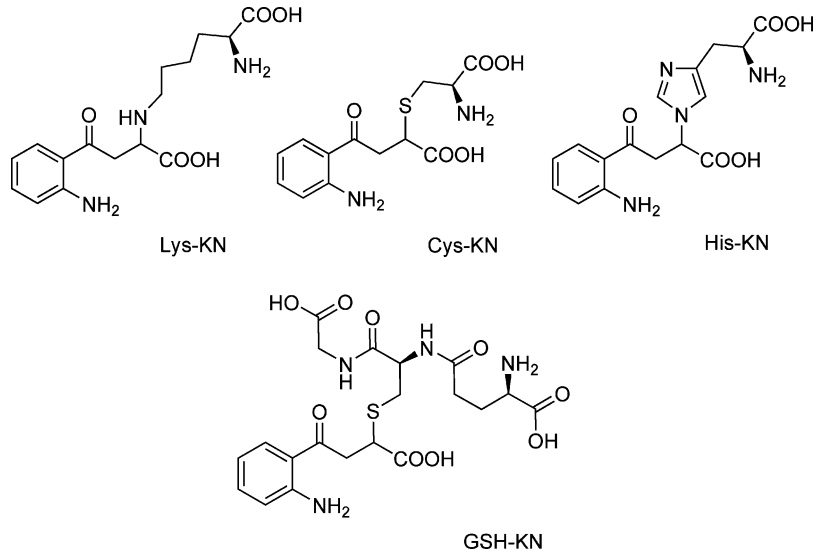

Hen egg white lysozyme (HEWL) was used as a model protein for this purpose. The chemical structures of Cys-KN, His-KN, Lys-KN, and GSH-KN are presented in Chart 1.

Experimental Methods

Materials. D,L-Kynurenine (KN), D,L-cysteine (Cys), *N*-acetyl-L-histidine (His), D,L-lysine (Lys), reduced L-glutathione (GSH), trifluoroacetic acid (TFA), and quinine bisulfate were used as received from Sigma/Aldrich. Sinapinic acid and α-cyano-4-hydroxycinnamic acid were used as received from Bruker Daltonics, Germany. Hen egg white lysozyme (HEWL) and dithiothreitol (DTT) were from Helicon, Russia; sequencing grade modified trypsin from Promega, USA. H_2O was doubly distilled. Deuterated water (D_2O), methanol (MeOH), ethanol (EtOH), *N*,*N*-dimethylformamide (DMF), and dimethylsulfoxide (DMSO) were used as received from Fluka. Acetonitrile (HPLC grade) was purchased from Cryochrom, Russia, and used as received.

The KN adducts of Cys, His, Lys, and GSH were synthesized according to the method described in ref 25: 33.3 mg of kynurenine sulfate salt were dissolved in 20 mL of phosphate buffer at pH 9.5, and the amino acids were added in 10-fold molar excess. The pH was readjusted to 9.5 with NaOH. The solution, placed in a glass vial, was bubbled with argon, sealed, and then incubated at 37 °C for 48 h. After adjusting the pH to 4.5 with hydrochloric acid, the reaction mixture was separated by semipreparative HPLC. The adduct-containing fractions were collected, lyophilized, and stored at 4 °C.

KN-modified lysozyme (m-HEWL) was prepared in two steps: first, CKA was synthesized, and second, HEWL was modified by CKA. For the CKA synthesis, the unbuffered aqueous KN solution (5 mM) was adjusted to pH 8.3 by dropwise addition of NaOH. The solution (volume 20 mL) was placed in a glass vial, bubbled with argon, capped, sealed with parafilm, and incubated at 70 °C. The pH of the solution was controlled with an Orion Research pH-meter with a glass electrode before and after incubation. CKA was isolated from the reaction mixture using semipreparative HPLC. For HEWL modification, 28.3 mg of HEWL was added to 11 mL of CKA-containing fraction; the pH was again adjusted to 8.6. The reaction mixture was incubated for 51 h at 37 °C, after which the protein fraction was isolated via dialysis against distilled water (pH 6.5) for 6 h at 4 °C, and finally was lyophilized and stored at 4 °C.

For the in-solution tryptic digests, 5 μg of HEWL and m-HEWL were dissolved in 10 μL of 8 M urea and incubated for 1 h at 60 °C. Afterward, 5 μL of 20 mM DTT was added and incubated for 30 min at 60 °C. To protect reduced cysteines from forming disulfide bonds over again, 5 μL of 50 mM iodoacetamide was added to the solution and stored at room temperature in the dark for 30 min. Before introducing trypsin to samples, 2 μL (0.5 mg/mL) of the enzyme was dissolved in 118 μL of 40 mM ammonium bicarbonate buffer. Then, 60 μL of the buffered trypsin solution was put into the HEWL and m-HEWL solutions and incubated overnight at 37 °C.

HPLC. Semipreparative HPLC separations were performed with the use of an Agilent LC 1100 chromatograph equipped with a UV−vis detector. Separations were carried out on a 9.4 × 250 mm ZORBAX Eclipse XBD-C18 column using an acetonitrile/0.05% (v/v) TFA in H_2O gradient. The adduct separations were performed with the gradients 0% (0−5 min), 0−50% (5−25 min), 50−100% (25−26 min), and 100% (26−30 min); the flow rate was 3.0 mL/min. CKA separations were performed with the gradients 0% (0−3 min), 0−30% (3−5 min), 30−55% (5−35 min), 55−100% (35−37 min), and 100% (37−40 min) at a flow rate of 1.0 mL/min.

Mass-Spectrometry Analysis. The mass spectra were obtained with a MALDI-TOF/TOF spectrometer Ultraflex III (Bruker Daltonics, Germany). In all experiments, a standard MTP ground steel plate (Bruker Daltonics, Germany) was used. The mass spectra of HEWL and m-HEWL were recorded in linear positive mode in the 3000−20000 *m*/*z* range; the mixture of 0.5 μL of concentrated and purified by Zip Tip pipet tips (Millipore, USA) protein solution and 0.5 μL of sinapinic acid solution (70% acetonitrile, 0.1% TFA) was dried under air. The mass spectra of HEWL and m-HEWL tryptic digests were recorded in reflective positive mode in the 500−4200 *m*/*z* range; the mixture of 0.5 μL of concentrated and purified by Zip Tip pipet tips protein digests and 0.5 μL of α-cyano-4-hydroxycinnamic acid (70% acetonitrile, 0.1% TFA) was dried in the air. MS/MS spectra of the peptides were recorded from the same spots on the plate as for MS spectra using the LIFT technology of the spectrometer; briefly, the daughter ions were generated using the increase of kinetic energy of parent ions with the subsequent fragmentation. First, the parent ion was chosen from

the mass spectrum of the digest. Second, the value of the chosen ion was declared as a parent mass in LIFT mode, and the MS spectrum of the isolated parent ion followed by the MS/MS spectrum of daughter ions was recorded. The detection of daughter ions was performed with standard built-in parameters; the registered *m/z* range was from 40 Da to the parent mass +20%.

Steady-State UV−vis Measurements. Steady-state absorption and fluorescence spectra were measured with a Cary 50 (Varian) spectrophotometer and a Cary Eclipse (Varian) fluorometer, respectively. All fluorescence spectra were corrected for the wavelength-dependent sensitivity of the detection. All solutions were deoxygenated by argon bubbling for 15 min prior to measurements, capped, and sealed with parafilm. The fluorescence quantum yields were determined relatively to a 1.0 N H_2SO_4 aqueous solution of quinine bisulfate (fluorescence quantum yield $\Phi_F = 0.546$ at 365 nm excitation[26]). For all measurements, a 10 × 10 mm^2 quartz cell was used and the absorbance of the samples was below 0.1 at the absorption maximum.

Time-Resolved Fluorescence Measurements. The early fluorescence dynamics was measured using the fluorescence upconversion setup described in detail elsewhere.[27] Briefly, part of the output of a mode locked Ti:sapphire oscillator (Spectra Physics "Tsunami") was frequency doubled and used to excite the sample at 400 nm. The fluorescence was gated by sum-frequency mixing with the fundamental of the oscillator output. The up-converted UV photons were directed into a monochromator and detected by a photomultiplier tube with photon counting electronics. The sample solutions were kept in a 1.0 mm thick spinning cell. The concentration was adjusted so that the absorbance of the sample was around 0.15 at the excitation wavelength. The full width at half-maximum (fwhm) of the instrument response function was around 210 fs.

Time-Correlated Single Photon Counting (TC-SPC) Measurements. Time profiles longer than 1 ns were measured using the TC-SPC unit described in ref 28. A pulsed laser diode at 395 nm (Picoquant model LDH-P-C-400B) with a repetition rate of 20 MHz was used for excitation; a MCP-PMT Hamamatsu R3809U-51 was used as a photomultiplier. The fwhm of the instrument response function was around 60 ps. A 10 × 10 mm^2 quartz cell was used, and the absorbance at 395 nm was about 0.1.

Transient Absorption (TA) Measurements. The experimental setup for pump−probe transient absorption (TA) has been described in detail elsewhere.[29] Excitation was performed at 400 nm using the frequency-doubled output of a standard 1 kHz amplified Ti:sapphire system (Spectra-Physics). The pump intensity on the sample was around 3 μJ. Probing was achieved with a white-light continuum obtained by focusing a small fraction of the 800 nm pulses into a CaF_2 plate. The polarization of the probe pulses was at magic angle relative to that of the pump pulses. All spectra were corrected for the chirp of the white light probe pulses. The fwhm of the instrument response function was ca. 200 fs. The sample solutions were placed in a 1 mm thick quartz cell where they were continuously stirred by N_2 bubbling. Their absorbance at the excitation wavelength was around 0.15. All time-resolved measurements were carried out at room temperature.

Laser Flash Photolysis (LFP) Measurements. A detailed description of the LFP equipment has been published earlier.[30,31] The solutions, placed in a square cell (inner dimensions 10 mm ×10 mm), were irradiated with a Quanta-Ray LAB-130-10 Nd:YAG laser (pulse duration 8 ns; 355 nm; pulse energy up to 150 mJ). The spot size of the laser beam at the cell entrance was 2.5 × 8 mm^2. The monitoring system includes a DKSh-150 xenon short-arc lamp connected to a high current pulser, a homemade monochromator, a 9794B photomultiplier (Electron Tubes Ltd.), and a LeCroy 9310A digitizer. The monitoring light, concentrated in a 2.5 × 1 mm^2 rectangle, passed through the cell along the front (laser irradiated) window. Thus, in all experiments the excitation optical length was 1 mm and the monitoring optical length was 8 mm. All solutions were bubbled with argon or oxygen for 15 min prior to, and during, irradiation.

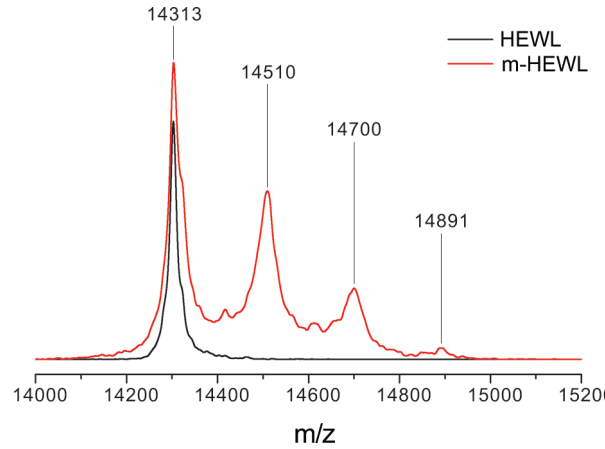

Figure 1. Mass spectra of HEWL and m-HEWL.

Results

Mass-Spectrometry Analysis of m-HEWL. The mass spectra of lysozyme (HEWL) and KN-modified lysozyme (m-HEWL) are presented in Figure 1. The strongest signal with *m/z* 14313 observed in the m-HEWL spectrum reveals the presence of unmodified protein in solution; the signals separated from the main peak by n*191 ± 4 Da correspond to proteins modified by one ($n = 1$), two ($n = 2$), and three ($n = 3$) deaminated KN molecules.

In order to determine the sites of the modification, HEWL and m-HEWL were subjected to the tryptic digestion. The mass spectrum of the peptides obtained from m-HEWL is presented in Figure 2a. The analysis of the spectrum reveals three peaks with *m/z* 797, 2528, and 2869, which were not present in the spectrum of the HEWL digest. These signals are separated by 191 Da from the peaks with *m/z* 606 (KVFGR), 2337 (NLCNIPCSALLSSDITASVNCAK), and 2678 (GYSLGNWVCAAKFESNFNTQATNR) observed in both HEWL and m-HEWL spectra and correspond to KN-modified peptides. It should be noted that each mentioned peptide contains a lysine amino acid residue, a possible site for KN attachment.[10,15]

Figure 2b depicts the MS/MS spectrum of the *m/z* 797 signal. The intense peak with *m/z* 606 corresponds to the peptide KVFGR, formed by the loss of the KN fragment. Less intense MS/MS peaks with *m/z* 175, 232, 379, and 478 correspond to y-ions of the KVFGR peptide. The signals from b-ions (*m/z* 129, 228, 375, 432, 588) are much weaker, which probably indicates the localization of the positive charge on the C-terminus of the peptide. The attachment of KN to the lysine residue (K1 of HEWL) is confirmed by the presence of a signal with *m/z* 320 corresponding to a b-ion of K-KN; no signals from b-ions of KV-KN, KVF-KN, and KVFG-KN fragments were found in the MS/MS spectrum.

A similar MS/MS analysis was also performed for the *m/z* 2869 ion (data not shown). The MS/MS spectrum contains an

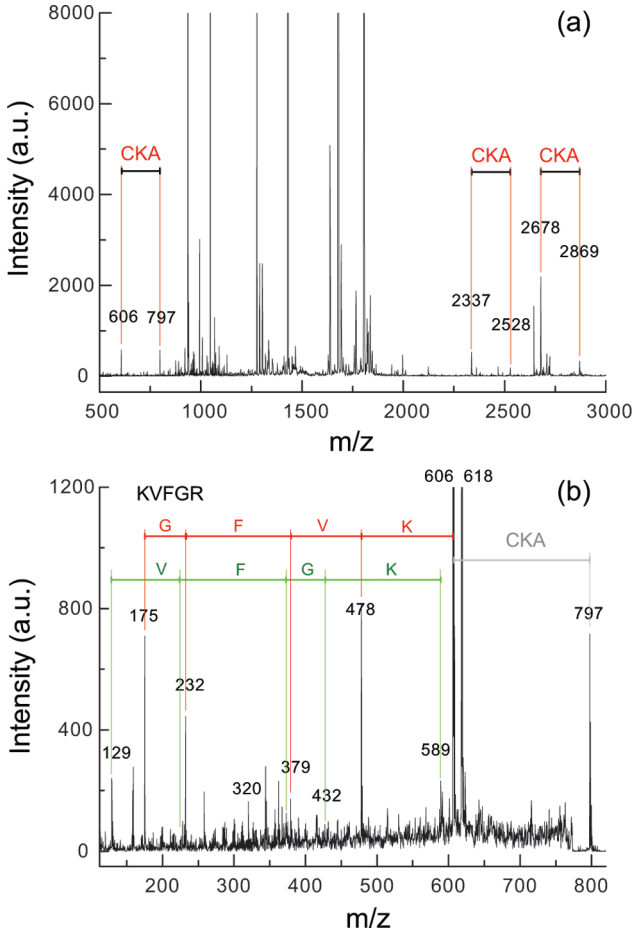

Figure 2. (a) Mass spectrum of m-HEWL after tryptic digestion. (b) MS/MS spectrum of the 797 *m/z* ion of hydrolyzed m-HEWL.

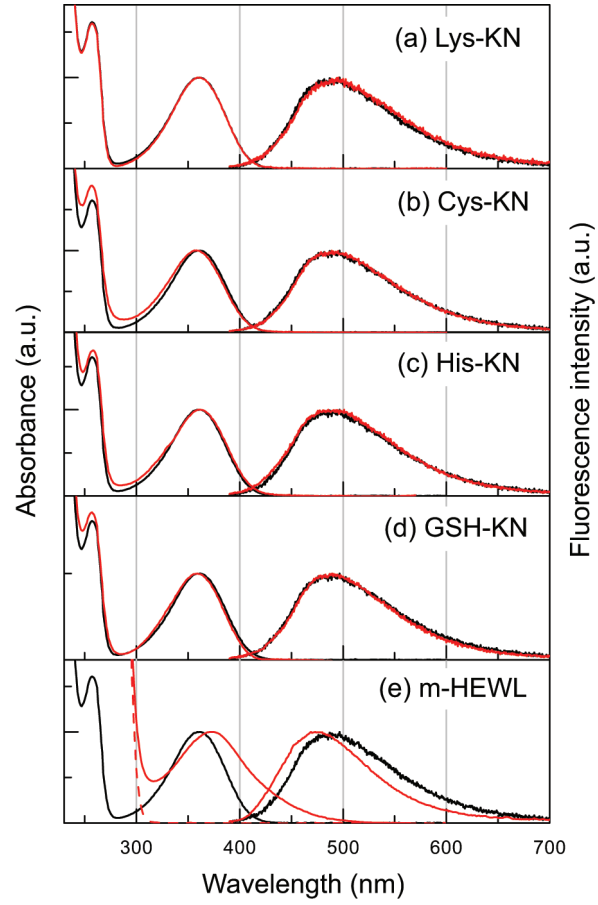

Figure 3. UV−vis absorption and fluorescence spectra of (a) Lys-KN, (b) Cys-KN, (c) His-KN, (d) GSH-KN, and (e) HEWL (dashed line) and m-HEWL (solid line) in neutral aqueous solution at room temperature. Red lines, compounds under study; black lines, KN in neutral aqueous solution.

intense signal with *m/z* 2678 corresponding to the GYSLGNWVCAAKFESNFNTQATNR peptide formed by the loss of the KN fragment. This sequence contains a K−F bond (lysine−phenylalanine), which was not hydrolyzed by trypsin likely due to the presence of the KN modification on the lysine residue (K33 of lysozyme). Furthermore, the signals from y-ions are present in the spectrum only until *m/z* 1428, which corresponds to the fragments of the FESNFNTQATNR peptide up to the lysine amino acid. Heavier y-ions containing lysine with probable modification are not detected.

The MS/MS spectrum of the *m/z* 2528 ion has not been recorded due to the low intensity of this signal. Summarizing the mass-spectrometric analysis, at least three positions in m-HEWL are modified by KN, and at least two of them are proved to be the lysine residues, namely, K1 and K33.

UV−vis Absorption Spectra and Fluorescence Quantum Yields. Figure 3a−d shows the UV−vis absorption and fluorescence spectra of Lys-KN, Cys-KN, His-KN, and GSH-KN (red lines) and KN (black lines) in neutral aqueous solution, pH 6.6. The differences in peak positions and spectral shapes between KN and its adducts are negligible. The spectra obtained with these compounds in organic solvents (MeOH, EtOH, DMF, and DMSO) are also very similar to each other (data not shown). The solvent-induced changes in the optical spectra of the adducts follow those observed with KN: a weak blue shift of the absorption band and a relatively large red shift of the fluorescence band when passing from aprotic to protic solvents.[23] These observations show a minor influence of the substituent on the spectral properties of KN.

The fluorescence quantum yields Φ_F of Lys-KN, Cys-KN, His-KN, and GSH-KN in various solvents are summarized in Table 1. In aqueous solutions, the Φ_F values of the adducts increase in the following order: Lys-KN, Cys-KN, His-KN, GSH-KN. For the Lys-KN adduct, the Φ_F value is similar to that for KN, whereas for GSH-KN it is twice as high. The increase of Φ_F from Lys-KN to GSH-KN can be observed in all protic solvents (D_2O, MeOH, and EtOH). In the aprotic solvents DMF and DMSO, the Φ_F values of the adducts are close to those of KN.

Figure 3e shows the UV−vis absorption and fluorescence spectra of m-HEWL in neutral aqueous solution (pH 5.8). Both the absorption and fluorescence bands of the protein-bound KN are shifted with respect to the spectra of KN aqueous solution, which may be attributed to the less protic and less polar local environment of the protein in comparison with the bulk solution. In fact, the m-HEWL fluorescence spectrum in H_2O is similar to the fluorescence spectrum of KN in MeOH,[23] which confirms this suggestion. Besides, the m-HEWL absorption band is broader than that of KN in MeOH; that agrees with the presence of several sites of KN attachment to HEWL. The average number of KNs attached to a protein molecule has been evaluated in the following way: the concentration of the protein dissolved in the sample was determined with use of the Bradford protein assay.[32] The concentration of KN in the sample was estimated by the absorption at 370 nm, assuming the extinction coefficient of KN attached to the protein to be the same as that of free KN, $\varepsilon_{370} = 4500\ M^{-1}\ cm^{-1}$.[8] The

TABLE 1: Photophysical Properties of KN and Its Adducts to Lysine (Lys-KN), Cysteine (Cys-KN), Histidine (His-KN), and Glutathione (GSH-KN) in Various Solvents at Room Temperature*

solvent	compound	Φ_F, %	τ_1, ps	τ_2, ps	τ_3, ps	k_F, s^{-1}	k_{NR}, s^{-1}
H_2O ($\alpha = 1.17$)	KN	0.08	0.9[a]	4.5[a]	27[a]	3.0×10^7	3.7×10^{10}
			1.0[b]	5.4[b]	26[b]		
	Lys-KN	0.07	1.1[a]	4.7[a]	28[a]	2.6×10^7	3.6×10^{10}
			1.1[b]	4.2[b]	29[b]		
	Cys-KN	0.12	0.9[a]	8.5[a]	44[a]	2.7×10^7	2.3×10^{10}
			1.3[b]	9.5[b]	41[b]		
	His-KN	0.15	1.2[a]	6.4[a]	48[a]	3.1×10^7	2.1×10^{10}
			1.5[b]	8.5[b]	49[b]		
	GSH-KN	0.15	1.3[a]	7.2[a]	47[a]	3.3×10^7	2.1×10^{10}
			1.1[b]	8.8[b]	46[b]		
D_2O	KN	0.14	1.2[a]	6.6[a]	43[a]	3.1×10^7	2.3×10^{10}
	Lys-KN	0.11	1.4[a]	8.1[a]	45[a]	2.4×10^7	2.2×10^{10}
			1.3[b]	6.1[b]	46[b]		
	Cys-KN	0.24	1.2[a]	11[a]	71[a]	3.4×10^7	1.4×10^{10}
			1.8[b]	14[b]	73[b]		
	His-KN	0.26	1.5[a]	10[a]	85[a]	3.1×10^7	1.2×10^{10}
			2.3[b]	15[b]	98[b]		
	GSH-KN	0.24	1.7[a]	15[a]	87[a]	3.1×10^7	1.3×10^{10}
			1.7[b]	12[b]	78[b]		
MeOH ($\alpha = 0.93$)	KN	0.79			240[c]	3.3×10^7	4.1×10^9
	Lys-KN	0.65	4.7[b]	21[b]	170[b]	3.8×10^7	5.8×10^9
					170[c]		
	Cys-KN	1.23	4.6[b]	26[b]	280[b]	4.3×10^7	3.4×10^9
					290[c]		
	His-KN	1.10	5.1[b]	26[b]	300[b]	3.6×10^7	3.2×10^9
					310[c]		
	GSH-KN	1.38	4.0[b]	34[b]	380[b]	3.6×10^7	2.6×10^9
					380[c]		
EtOH ($\alpha = 0.83$)	KN	2.3			480[c]	4.8×10^7	2.0×10^9
	Lys-KN	1.3	not measured	not measured	360[c]	3.6×10^7	2.7×10^9
	Cys-KN	2.5			670[c]	3.7×10^7	1.5×10^9
	His-KN	2.2			590[c]	3.7×10^7	1.7×10^9
	GSH-KN	3.7			790[c]	4.7×10^7	1.2×10^9
DMF ($\alpha = 0$)	KN	5.3			1400[c]	3.8×10^7	6.8×10^8
	Lys-KN	5.0	not measured	not measured	1350[c]	3.7×10^7	7.1×10^8
	Cys-KN	5.9			1350[c]	4.4×10^7	7.0×10^8
	His-KN	5.5			1450[c]	3.9×10^7	6.6×10^8
	GSH-KN	5.5			1050[c]	5.2×10^7	9.0×10^8
DMSO ($\alpha = 0$)	KN	9.0	3.3[a]	41[a]	2300[a]	4.0×10^7	4.0×10^8
			4.3[b]	52[b]	2400[b]		
	Lys-KN	9.3	5.6[b]	100[b]	1850[b]	5.1×10^7	5.0×10^8
					1800[c]		
	Cys-KN	10.3	4.3[b]	66[b]	1850[b]	5.6×10^7	4.9×10^8
					1850[c]		
	His-KN	9.8	8.7[b]	120[b]	1700[b]	5.6×10^7	5.2×10^8
					1750[c]		
	GSH-KN	7.8	6.6[b]	72[b]	1500[b]	5.3×10^7	6.2×10^8
					1500[c]		

* α, Kamlet−Taft's solvatochromic parameter characterizing the hydrogen-bonding ability of the solvent;[35,36] τ_i, time constants obtained from the fits of (a) fluorescence up-conversion, $\lambda_{ex} = 400$ nm, (b) TA, $\lambda_{ex} = 400$ nm, or (c) TC-SPC, $\lambda_{ex} = 395$ nm, measurements (see the superscript letters in the table); Φ_F, fluorescence quantum yield; k_F and k_{NR}: radiative and non-radiative rate constant. Standard error: 10%.

TABLE 2: Fluorescence Properties of m-HEWL in Aqueous Solvents at Room Temperature*

solvent	Φ_F, %	τ_1, ps	τ_2, ps	τ_3, ps	τ_4, ns	τ_5, ns
H_2O (pH 5.7)	0.54	0.9 (0.20)[a]	34 (0.36)[a]	360 (0.44)[a]		
		1.0[b]	52[b]	640[b]		
				380 (0.72)[c]	2.0 (0.25)[c]	12 (0.03)[c]
D_2O	1.00			460 (0.57)[c]	2.7 (0.36)[c]	9.5 (0.07)[c]

* Φ_F, fluorescence quantum yield; τ_i, time constants obtained from fits of (a) fluorescence up-conversion, $\lambda_{ex} = 400$ nm, (b) TA, $\lambda_{ex} = 400$ nm, or (c) TC-SPC, $\lambda_{ex} = 395$ nm, measurements. (See the superscript letters in the table. Data in parentheses show the amplitude factors of the temporal components.) Standard error: 10%.

concentration ratio [KN]/[m-HEWL] gives a value of 1.6. Thus, the investigated m-HEWL represents a mixture of unmodified proteins and proteins mainly modified by one and two KN molecules, that is in agreement with the mass-spectrometry data (see Figure 1).

The fluorescence quantum yields of m-HEWL were measured in nonbuffered H_2O and D_2O; the obtained values are listed in Table 2. In aqueous solutions, m-HEWL exhibits a 7-fold higher fluorescence quantum yield than KN; the measurements in D_2O clearly indicate the presence of an isotopic effect. No differences

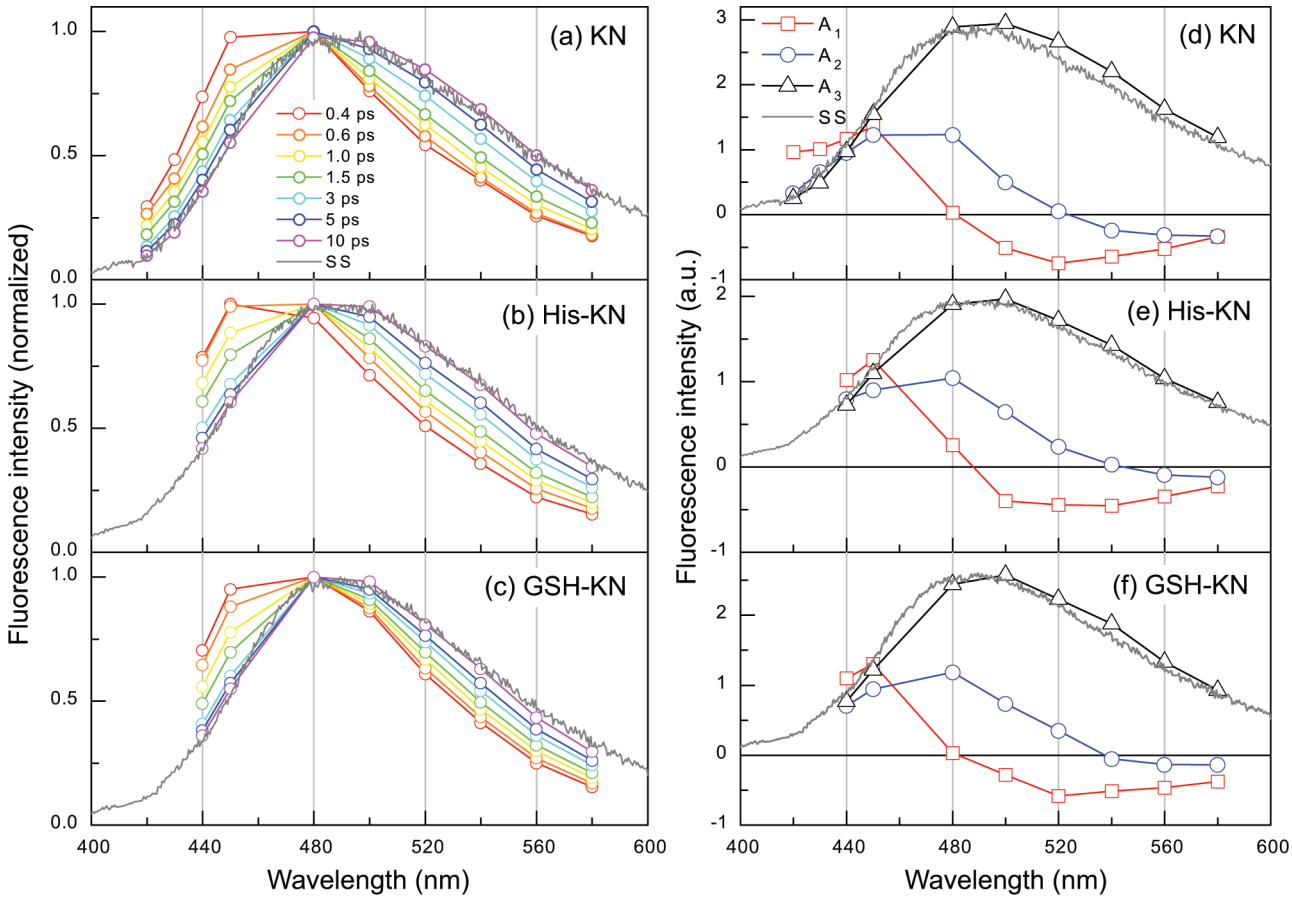

Figure 4. (a−c) Intensity normalized time-resolved fluorescence spectra of (a) KN, (b) His-KN, and (c) GSH-KN observed after 400 nm excitation. (d−f) Decay-associated amplitude spectra obtained from the global analysis of the fluorescence time profiles measured with (d) KN, (e) His-KN, and (f) GSH-KN. Gray lines: steady-state fluorescence spectra.

in the spectral properties or fluorescence quantum yield of m-HEWL were observed between buffered and nonbuffered solutions.

Ultrafast Excited State Dynamics of Lys-KN, Cys-KN, His-KN, and GSH-KN. The temporal evolution of Lys-KN, Cys-KN, His-KN, and GSH-KN fluorescence in H_2O (pH 6.6) has been measured at eight equidistant wavelengths from 420 to 580 nm throughout the emission band over different time windows up to 300 ps. The dynamics for all adducts qualitatively reproduce the one found for KN: an initial red shift of the emission band, induced by solvent relaxation (so-called dynamic Stokes shift), is followed by a monotonic decay.[23] This spectral dynamics can be clearly seen in Figure 4a−c. The main difference in the emission dynamics between KN and its adducts is a faster signal evolution in the case of KN (Figure 5a).

The measured fluorescence data were treated by global analysis using a sum of exponential functions convolved with a Gaussian-like instrument response function, as described in detail in refs 33 and 34. For all adducts, a good agreement between experimental and calculated data was obtained with three exponentials. The time constants obtained from such analysis are listed in Table 1. Figure 4d−f shows the wavelength dependence of the amplitude factors associated with the various time constants, $A_1(\lambda)$, $A_2(\lambda)$, and $A_3(\lambda)$, obtained from the global analysis with KN, His-KN, and GSH-KN. Positive values correspond to a decay, negative ones to a rise. The spectra associated with the fast components, $A_1(\lambda)$ and $A_2(\lambda)$, exhibit a similar shape, indicating a decay on the high-energy side and a rise on the low-energy side. These components can thus be

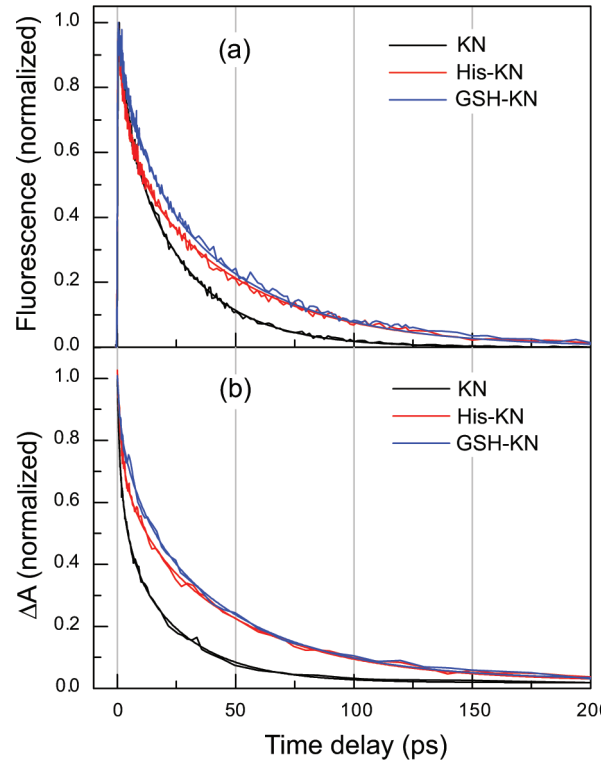

Figure 5. (a) Fluorescence and (b) TA time profiles recorded with KN, His-KN, and GSH-KN at the emission maximum, 500 nm, and at the TA band maximum, 570 nm, correspondingly.

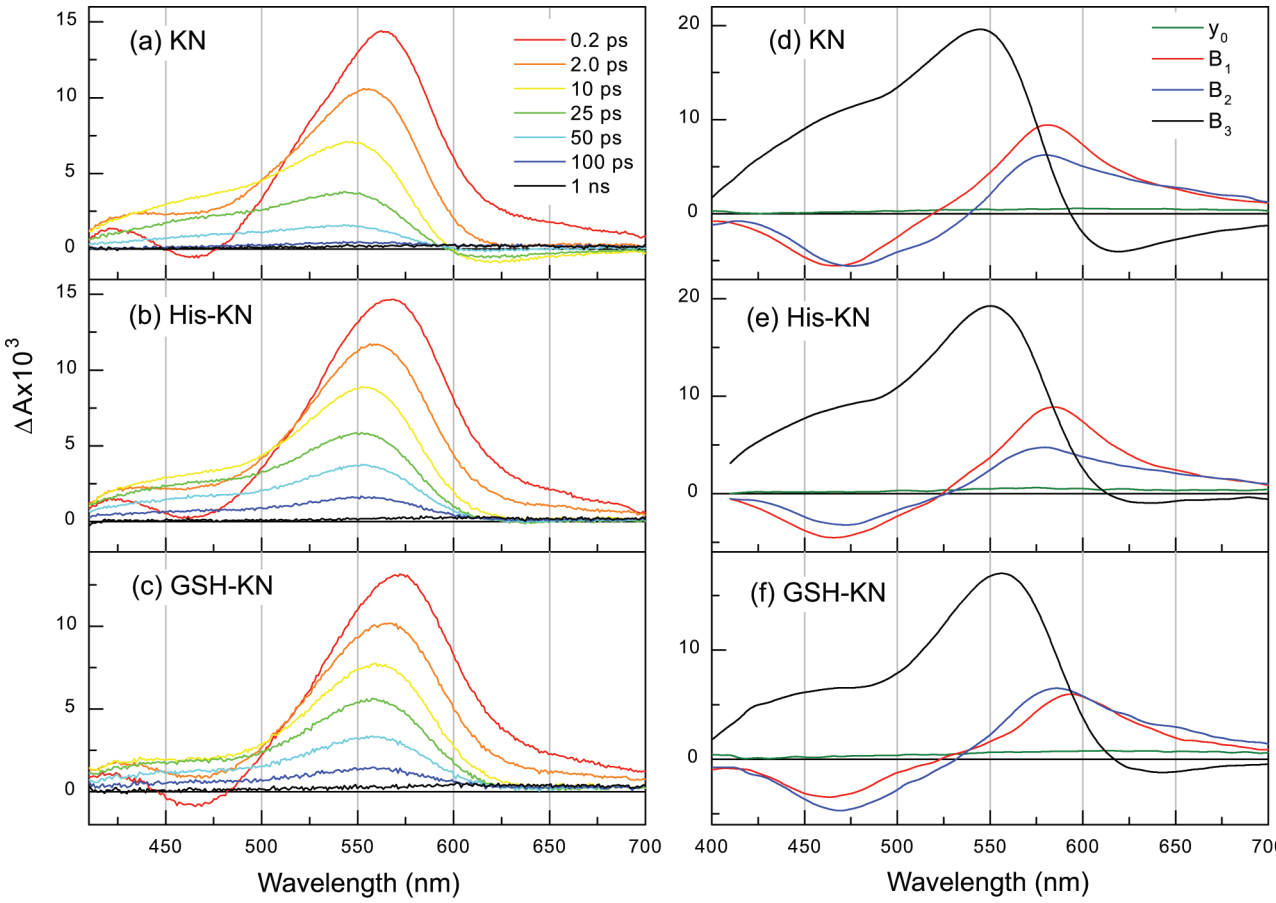

Figure 6. (a−c) TA spectra recorded at different time delays after 400 nm excitation of (a) KN, (b) His-KN, and (c) GSH-KN. (d−f) Decay-associated amplitude spectra obtained from the global analysis of the TA spectra of (d) KN, (e) His-KN, and (f) GSH-KN.

attributed predominantly to a dynamic Stokes shift. The amplitude factors $A_3(\lambda)$ related to the largest time constant almost coincide with the steady-state emission spectrum (thin gray line). Thus, the time constant τ_3 can be assigned to the lifetime of the lowest singlet excited state.

TA spectra of KN adducts in aqueous solutions (pH 6.6) were recorded upon 400 nm excitation, some of them being shown in Figure 6a−c. As in the case of fluorescence, the TA dynamics of all adducts are similar to that of KN: a solvent-induced red shift of the stimulated emission band leads to a blue shift of the resulting TA band. The disappearance and appearance of the negative bands around 470 nm and at $\lambda > 600$ nm, respectively, should also be related to the dynamic Stokes shift of the stimulated emission band. The decay dynamics of the TA signal at 570 nm are slower for all adducts compared with KN, and they reproduce well the fluorescence data (Figure 5b).

A global analysis of the TA spectra was performed with the sum of three exponential functions and gave the characteristic times presented in Table 1, which are similar to those obtained from the fluorescence measurements. The decay associated spectra, $B_1(\lambda)$, $B_2(\lambda)$, and $B_3(\lambda)$, are shown in Figure 6d−f. The spectra associated with the fast components, $B_1(\lambda)$ and $B_2(\lambda)$, are similar to those of the $A_1(\lambda)$ and $A_2(\lambda)$ amplitudes in the fluorescence measurements but have opposite signs (Figure 4d−f). $B_3(\lambda)$ corresponds to the superposition of the $S_1 \rightarrow S_n$ absorption and $S_1 \rightarrow S_0$ stimulated emission bands. The negative feature above 600 nm is due to the red shift of the stimulated emission. Thus, the TA results are completely consistent with the time-resolved fluorescence data, and τ_3 in Table 1 can be assigned to the excited state lifetime of the KN adducts.

The same fluorescence upconversion and TA measurements were carried out in D_2O, and TA measurements were also performed in MeOH and DMSO. The characteristic time constants obtained from the analysis of the fluorescence and absorption data as described above are listed in Table 1. In deuterated water, the excited-state dynamics of all adducts is slowed down by a factor of approximately 1.5 compared to H_2O, whereas the shapes of the fluorescence and TA spectra remain the same. These observations indicate a substantial participation of intermolecular hydrogen bonds in the ultrafast deactivation of the excited states of the adducts. The spectral evolution of the TA signals of all adducts in MeOH and DMSO qualitatively repeats that of KN.[23] As in the case of KN, the observed dynamics with all adducts includes three stages and the corresponding time constants increase from MeOH to DMSO (Table 1).

The fluorescence lifetimes of the adducts in MeOH, EtOH, DMF, and DMSO were obtained using the TC-SPC technique. The temporal evolution of the emission measured at 500 nm exhibits an exponential decay in all solvents (data not shown). The decay times were obtained using the numerical convolution of the experimental instrument response function with a monoexponential function. The resulting fluorescence lifetimes of the adducts in different solvents are assigned to the S_1 state lifetimes (τ_3) and are summarized in Table 1. The obtained lifetimes agree well with the results obtained from the TA experiments.

The obtained Φ_F and τ_3 values (Table 1) were used to calculate the rate constants of radiative and nonradiative decay of the excited state. The k_F values amount to about (3−5) ×

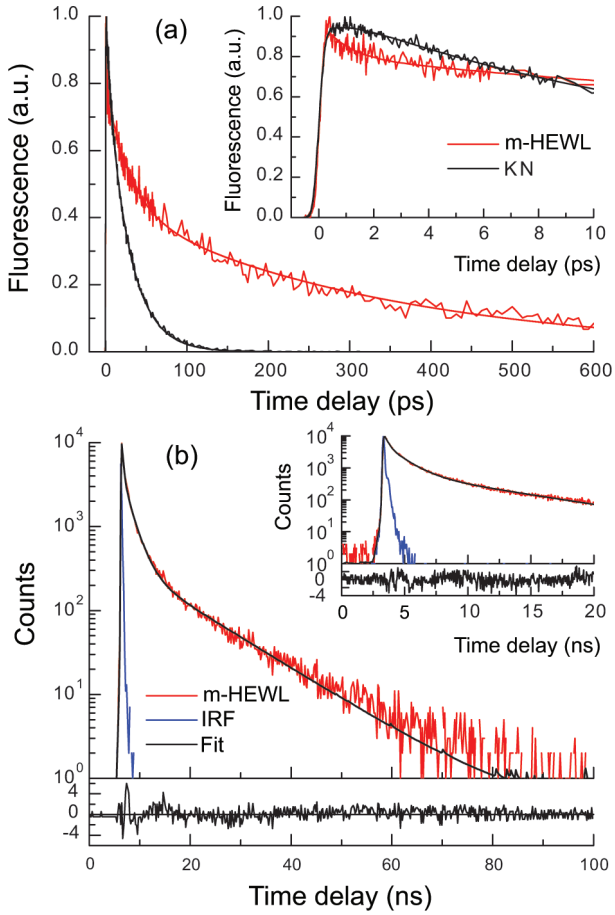

Figure 7. Fluorescence time profiles of m-HEWL aqueous solutions (pH 5.7) recorded on (a) picosecond (at the maximum of emission, 480 nm) and (b) nanosecond time scales (at 540 nm). Black lines in part a: the time profile of KN aqueous solution (pH 6.6) recorded at the maximum of emission, 500 nm. Insets: the early dynamics at the same wavelengths.

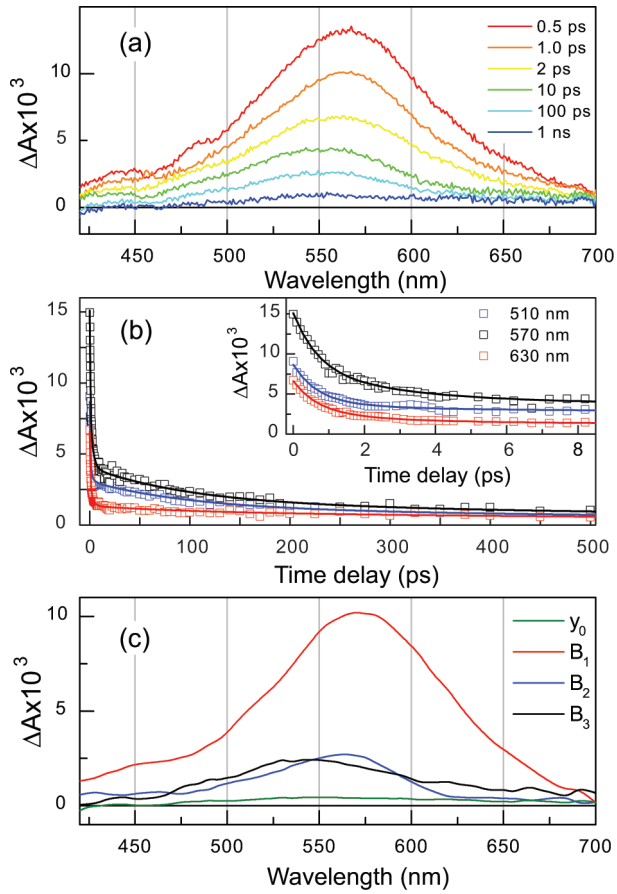

Figure 8. TA dynamics of m-HEWL aqueous solution (pH 5.7) observed after 400 nm excitation. (a) TA spectra recorded at different time delays after excitation. (b) TA time profiles measured at 510, 570, and 630 nm; solid lines show best fit; inset shows early dynamics at the same wavelengths. (c) Decay-associated amplitude spectra obtained from the global analysis of the TA time profiles.

10^7 s^{-1} and depend weakly on the solvent (see Table 1), whereas the k_{NR} values for KN and adducts increase by 2 orders of magnitude from DMSO to H_2O. The drastic increase of k_{NR} in protic solvents correlates with the increase of the hydrogen-bonding ability of these solvents, which can be quantified by the Kamlet−Taft's solvatochromic parameter α[35,36] shown in Table 1.

Ultrafast Excited State Dynamics of m-HEWL. The temporal evolution of m-HEWL fluorescence in aqueous solution (pH 5.7) has been measured at three wavelengths (480, 500, and 520 nm) over different time windows up to 600 ps. Figure 7a shows the fluorescence time profiles of m-HEWL and KN at the maxima of their emission bands, 480 and 500 nm, respectively. The fluorescence dynamics of m-HEWL is significantly slower than that of KN. The early dynamics, displayed in the inset in Figure 7a, shows that m-HEWL fluorescence intensity exhibits only a decay, while KN shows a growing signal due to solvent relaxation. It should be noted that no rising component was detected for m-HEWL at any wavelength. Taking into account that the measurements were performed at wavelengths corresponding to the low-energy side of the emission band, it might be concluded that the solvent relaxation dynamics is hidden by a fast process leading to a rapid decay of a part of the singlet excited state population. Additionally, solvent relaxation of m-HEWL can be expected to significantly differ from that of KN in aqueous solution due to the protein environment.

The measured time profiles were analyzed using the sum of three exponential functions convolved with a Gaussian-like instrument response function as described earlier. The best fit presented by a smooth line in Figure 7a was obtained with the following time constants: $\tau_1 = 0.9$ ps (amplitude factor 0.20), $\tau_2 = 34$ ps (0.36), and $\tau_3 = 360$ ps (0.44). Similar time constants were obtained for the time profiles recorded at 500 and 520 nm (data not shown). The assignment of the time constants will be discussed below.

Figure 7b displays the m-HEWL fluorescence dynamics in H_2O (pH 5.7) on a larger time scale recorded at 500 nm using TC-SPC, whereas the inset presents the early dynamics. The time profile was analyzed by the convolution of the sum of exponential functions with the experimental instrument response function. A good agreement between experimental and calculated data was obtained with three exponentials. The best fit, presented by smooth black lines in Figure 7b, was obtained with the time constants listed in Table 2. These time constants are designated as τ_3, τ_4, and τ_5, since the fastest component of the TC-SPC time profile and the slowest component of the upconversion time profile practically coincide. The fluorescence time profile of m-HEWL in D_2O was obtained in a similar way; the same fitting procedure gave the time constants summarized in Table 2.

Figure 8a shows TA spectra of m-HEWL in aqueous solution (pH 5.7) recorded upon 400 nm excitation. As in the case of KN and of the adducts, an absorption band with a maximum at 570 nm is immediately present after excitation. The early

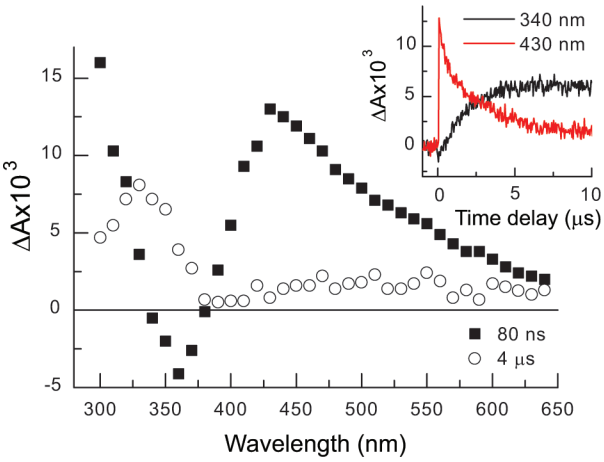

Figure 9. Transient absorption spectra detected 80 ns (filled squares) and 4 μs (open circles) after the laser pulse irradiation (355 nm, 70 mJ) of m-HEWL in argon saturated aqueous solution (pH 5.8) in the presence of 0.01 M acetone. Insets show the time profiles at 340 and 430 nm.

dynamics includes a fast decay and a minor blue shift of the absorption band (Figure 8a,b). The subsequent dynamics exhibits a monotonic decay with negligible changes in the spectral shape. The absence of negative features over the whole spectral window should be noted.

Global analysis of the TA dynamics was performed using the sum of three exponential functions, the best fit being obtained with time constants: $\tau_1 = 1.0$ ps, $\tau_2 = 52$ ps, and $\tau_3 = 640$ ps. The decay associated spectra, $B_1(\lambda)$, $B_2(\lambda)$, and $B_3(\lambda)$, are displayed in Figure 8c. All amplitudes show positive values over the whole spectral region; a blue shift of $B_3(\lambda)$ relative to $B_1(\lambda)$ and $B_2(\lambda)$ can be observed. Interestingly, the fastest component, $B_1(\lambda)$, gives the largest contribution to the observed dynamics (Figure 8c). The τ_1 values obtained from fluorescence and TA measurements coincide, but the τ_2 and τ_3 values exhibit a significant difference. Probably, this difference can be attributed to the weakness of the TA signal in the time range $t > 100$ ps, where the low signal/noise ratio results in a lower accuracy of the time constant.

Laser Flash Photolysis of m-HEWL. Figure 9 shows TA spectra obtained upon 355 nm photolysis of aqueous m-HEWL solution (1.3×10^{-4} M, pH 6.4) under argon 80 ns and 4 μs after the laser flash. The TA dynamics was recorded with a laser pulse energy of 70 mJ in order to minimize a contribution from the KN biphotonic ionization.[37] To exclude a contribution from the solvated electron, the well-known electron scavenger acetone was added to the solution. Immediately after the laser pulse, a positive TA band with the maximum at 430 nm and a negative TA band with the maximum at 360 nm are observed. The subsequent dynamics consists of a monotonic decay of the TA signal below 320 nm and above 380 nm, and of the build-up of a positive TA band with a maximum at 340 nm. The TA signal evolution over the whole wavelength region occurs with a rate constant of $(5 \pm 1) \times 10^5$ s^{-1}, and shows no dependence on the laser energy and concentration of m-HEWL, indicating an intramolecular character of the reaction. In the presence of oxygen, the decay of the TA signal is significantly accelerated and, after the completion of the signal decay, no absorption was observed over the whole wavelength region (data not shown). These observations allow an assignment of the positive absorption observed immediately after the laser flash to the triplet state of KN bound to the protein. Thus, the TA spectrum observed immediately after the laser pulse is a superposition of the KN triplet state absorption, which has absorption maxima at 280, 340, and 430 nm,[8,37] and of the depletion of the starting material, which has an absorption maximum at 370 nm (see Figure 3e).

The triplet yield of KN bound to protein was determined relatively to the free KN in solution. The initial TA values at 430 nm, ΔA_{430}, were measured for aqueous KN and m-HEWL solutions with the same optical densities at 355 nm (excitation wavelength) at different laser energies. The triplet yield of m-HEWL, $\Phi_T = 3.4 \pm 0.5\%$, was calculated from the ratio of the slopes of the linear fit of ΔA_{430} laser pulse energy dependencies (see the Supporting Information) and using KN triplet yield as a standard ($\Phi_T = 1.8\%$).[8]

The intramolecular character of ^{T}KN quenching stimulated the search for probable quenchers among the aromatic amino acid residues present in lysozyme. The most probable quenchers of triplet KN are tryptophan and tyrosine residues, both of which being able to quench ^{T}KN via electron transfer reaction.[24] As a consequence, the absorption band with a maximum at 330 nm, observed 4 μs after laser pulse excitation of m-HEWL in aqueous solution (Figure 9), can be attributed to the absorption of Trp$^\bullet$ radical (absorption bands at 330 and 510 nm)[38−40] formed upon the deprotonation of the TrpH$^{\bullet+}$ radical ($pK_a = 4.3$,[38] absorption bands at 330 and 570 nm[38,39,41]). However, we could not observe any growing transient absorption signals corresponding to the radical formation at 510 nm (the maximum of Trp$^\bullet$ radical) or at 410 nm (the maximum of Tyr$^\bullet$ radical),[42,43] probably because of the overlap of radical absorption with the broad absorption band of ^{T}KN.

Analysis of a m-HEWL solution after irradiation revealed the presence of 4-hydroxyquinoline (4HQN) and KN yellow, the products of KN photochemical and thermal degradation.[11,12,44] Thus, one of the possible channels of m-HEWL photodecomposition is the detachment of KN followed by cyclization with the formation of 4HQN and KN yellow. The detailed mechanism of these processes is unclear and can include both thermal and photochemical stages, including biphotonic reactions.

Discussion

Photophysics of the KN Adducts. The fluorescence and transient absorption dynamics of all adducts in various solvents are qualitatively similar to those of KN. Therefore, the same interpretation can be proposed for the time constants: the time constant τ_1 can be assigned to the diffusive motion of the solvent around the excited molecule, τ_2 corresponds to conformational changes of the adduct in the excited state, and τ_3 can be attributed to the lifetime of the lowest singlet excited state.[23] The obtained τ_1 values agree with the data reported in literature for the same solvents;[45−47] the τ_2 and τ_3 values exhibit a monotonic increase from Lys-KN to GSH-KN and from protic to aprotic solvents. The increase of the time constant τ_2 from KN to GSH-KN correlates with the increase of the molecular size, which agrees with its assignment to conformational relaxation.

The observed isotopic effect and the strong solvent dependence of τ_3 point to a solvent-assisted mechanism of the excited state deactivation for all the adducts under study. The increase of τ_3 from Lys-KN to GSH-KN in protic media indicates a decrease of the efficiency of the deactivation mechanism. It seems likely that the presence of a substituent comparable in size with KN leads to a weakening and/or blocking of intermolecular hydrogen bonds between the chromophoric moiety of the adduct and the solvent molecules. As a result, a slowing down of the radiationless $S_1 \rightarrow S_0$ transition occurs. In aprotic media, where intermolecular hydrogen bonds are absent,

the lifetimes and quantum yields of fluorescence are similar for KN and all the adducts. A small decrease of the fluorescence lifetime and quantum yield from Cys-KN to GSH-KN in DMSO (Table 1) should be noticed: it might be due to intramolecular hydrogen bonding between the aminoacetophenone moiety and the Cys, His, and GSH substituents.

Photophysics and Photochemistry of m-HEWL. The fluorescence and absorption dynamics of m-HEWL reveal a multiphasic decay of the singlet excited state population of KNs covalently attached to HEWL. This dynamics is most probably due to KNs bound to different sites of the protein. The fastest component exhibits a time constant close to a characteristic time for solvent relaxation in aqueous solution;[45−47] however, the dynamic Stokes shift is strongly suppressed by the fast decay (Figures 7 and 8). A reaction between the S_1 state of the bound KN and neighboring amino acid residues via an electron transfer can be suggested. In this case, transient bands from kynurenine radicals with an absorption maximum at 430 nm[24] should be observed. The absence of any long-lived signal in this region (Figure 8a) points to a fast charge recombination. Considering the structure of HEWL,[48] the possible quenchers of the photoexcited KNs bound to m-HEWL might be F3 (phenylalanine) and F38 residues located in the immediate proximity of K1 and F3, F34, F38, and W123 (tryptophan) which are close to K33. Unfortunately, our data do not allow the mechanism of this ultrafast reaction, which represents a very efficient deactivation channel of the KN S_1 state, to be fully established.

The second, third, and fourth components of the excited-state dynamics could be assigned to excited KNs that do not have a suitable electron donor in a nearest environment. The obtained τ_2 value is close to the S_1 state lifetime of KN adducts in water; the τ_3 time constant is similar to the fluorescence lifetime of the adducts in EtOH; the τ_4 value to the KN fluorescence lifetime in aprotic solvents (see Table 1). Apparently, these time constants could be associated with KNs attached to different amino acid residues and having different access to solvent molecules: the higher τ values correspond to KNs with weaker exposure to water molecules. Thus, τ_2 might be attributed to KNs located at the outer surface of m-HEWL, τ_3 to KNs partially buried in the protein globule, and τ_4 to KNs deeply inside the protein globule. The largest time constant (τ_5) observed in the TC-SPC experiment is at least 4 times higher than the fluorescence lifetime of KN in aprotic DMSO. Most likely, this component corresponds to impurities present in the solution. Thus, the excited state dynamics of m-HEWL reveals at least four components of KN excited state decay. Some of these components could also be attributed to the presence of several m-HEWL conformations where the same KN-modified residues are included in protein domains of different proticity.

The lifetime of the triplet state of m-HEWL is about 2 μs and does not depend on the laser pulse energy and on the m-HEWL concentration in solution: the triplet state is quenched by amino acid residues of the protein. The obtained data are not sufficient to determine the amino acid responsible for this quenching, although tryptophan residues seem to be the most probable candidates.

We have to note that the model protein used in the current work, lysozyme, differs from the lens proteins: crystallins have cysteine residues which are not coupled via disulfide bridges and therefore are open for modification by UV filters. Besides, crystallins have fewer aromatic amino acid residues, which can effectively quench the photoexcited states of covalently bound UV filters. Thus, UV filters attached to crystallins may demonstrate even higher photochemical activity. This will be the topic of our further investigations.

Conclusions

The results obtained in the present work demonstrate that the covalent attachment of the UV filter kynurenine to amino acids and proteins results in a significant increase of its photoactivity. The main reason of this effect is the decrease of the rate of solvent-assisted internal conversion, the major deactivation channel of the S_1 state. With aging, the concentrations of major UV filters in the human lens—3OHKN, AHBG, and KN—significantly decrease,[18] whereas the levels of GSH-3OHKN adduct and kynurenines attached to the lens proteins increase.[18] Thus, the susceptibility to UV light of the aged lens is much higher than that of the young one, which may give a significant contribution to the age-related cataract development.

Acknowledgment. This work was supported by the following agencies: FASI state contracts 02.512.11.2278, 02.740.11.0262, and P708, Russian Foundation for Basic Research (projects 08-03-00539 and 09-04-12135), Grant of the President of Russian Federation (grant NSh-7643.2010.3), the Division of Chemistry and Material Science, Russian Academy of Sciences, the SNF (Project Nr. 200020-124393), and the University of Geneva. P.S.S. thanks the European Scientific Foundation (DYNA Exchange Grant #1929).

Supporting Information Available: Laser pulse energy dependence of the initial absorption at 430 nm of m-HEWL and KN in neutral aqueous solutions. This material is available free of charge via the Internet at http://pubs.acs.org.

References and Notes

(1) van Heyningen, R. Fluorescent Glucoside in the Human Lens. *Nature* **1971**, *230*, 393–394.

(2) van Heyningen, R. *The Human Lens in Relation to Cataract. Ciba Foundation Symposium*; Elsevier: Amsterdam, The Netherlands, 1973; Vol. 19, pp 151−171.

(3) Wood, A. M.; Truscott, R. J. W. UV Filters in Human Lenses: Tryptophan Catabolism. *Exp. Eye Res.* **1993**, *56*, 317–325.

(4) Truscott, R. J. W.; Wood, A. M.; Carver, J. A.; Sheil, M. M.; Stutchbury, G. M.; Zhu, J.; Kilby, G. W. A New UV-filter Compound in Human Lenses. *FEBS Lett.* **1994**, *384*, 173–176.

(5) Dillon, J.; Atherton, S. J. Time Resolved Spectroscopic Studies of the Intact Human Lenses. *Photochem. Photobiol.* **1990**, *51*, 465–468.

(6) Krishna, C. M.; Uppuluri, S.; Riesz, P.; Zigler, J. S.; Balasubramanian, D. A Study of the Photodynamic Efficiencies of Some Eye Lens Constituents. *Photochem. Photobiol.* **1991**, *54*, 51–58.

(7) Reszka, K. J.; Bilski, P.; Chignell, C. F.; Dillon, J. Free Radical Reactions Photosensitized by the Human Lens Component, Kynurenine: an ESR and Spin Trapping Investigation. *Free Radical Biol. Med.* **1996**, *20*, 23–34.

(8) Tsentalovich, Yu.P.; Snytnikova, O. A.; Sherin, P. S.; Forbes, M. D. E. Photochemistry of Kynurenine, a Tryptophan Metabolite: Properties of the Triplet State. *J. Phys. Chem. A* **2005**, *109*, 3565–3568.

(9) Bova, L. M.; Wood, A. M.; Jamie, J. F.; Truscott, R. J. W. UV Filter Compounds in Human Lenses: the Origin of 4-(2-amino-3-hydroxyphenyl)-4-oxobutanoic Acid O-beta-D-Glucoside. *Invest. Ophthalmol. Visual Sci.* **1999**, *40*, 3237–3244.

(10) Kopylova, L. V.; Snytnikova, O. A.; Chernyak, E. I.; Morozov, S. V. Tsentalovich, UV Filter Decomposition. A Study of Reactions of 4-(2-amino-3-aminophenyl)-4-oxocrotonic Acid with Amino Acids and Antioxidants Present in the Human Lens. *Exp. Eye Res.* **2007**, *85*, 242–249.

(11) Taylor, L. M.; Aquilina, J. A.; Jamie, J. F.; Truscott, R. J. W. UV Filter Instability: Consequences for the Human Lens. *Exp. Eye Res.* **2002**, *75*, 165–175.

(12) Tsentalovich, Yu.P.; Snytnikova, O. A.; Forbes, M. D. E.; Chernyak, E. I.; Morozov, S. V. Photochemical and Thermal Reactivity of Kynurenine. *Exp. Eye Res.* **2006**, *83*, 1439–1445.

(13) Hood, B. D.; Garner, B.; Truscott, R. J. W. Evidence for Crystalline Modification by the Major Ultraviolet Filter, 3-Hydroxy-kynurenine *O*-β-D-Glucoside. *J. Biol. Chem.* **1999**, *274*, 32547–32550.

(14) Taylor, L. M.; Aquilina, J. A.; Jamie, J. F.; Truscott, R. J. W. Glutathione and NADH, but not Ascorbate, Protect Lens Proteins from Modification by UV Filters. *Exp. Eye Res.* **2002**, *74*, 503–511.

(15) Vazquez, S.; Aquilina, J. A.; Jamie, J. F.; Sheil, M. M.; Truscott, R. J. W. Novel Protein Modification by Kynurenine in Human Lenses. *J. Biol. Chem.* **2002**, *277*, 4867–4873.

(16) Korlimbinis, A.; Truscott, R. J. W. Identification of 3-Hydroxykynurenine Bound to Protein in the Human Lens. A Possible Role in Age-Related Nuclear Cataract. *Biochemistry* **2006**, *45*, 1950–1960.

(17) Garner, B.; Vazquez, S.; Griffith, R.; Lindner, R. A.; Carver, J. A.; Truscott, R. J. W. Identification of Glutathionyl-3-hydroxykynurenine Glucoside as a Novel Fluorophore Associated with Aging of the Human Lens. *J. Biol. Chem.* **1999**, *274*, 20847–20854.

(18) Bova, L. M.; Sweeney, M. H.; Jamie, J. F.; Truscott, R. J. W. Major Changes in Human Ocular UV Protection with Age. *Invest. Ophthalmol. Visual Sci.* **2001**, *42*, 200–205.

(19) Aquilina, J. A.; Truscott, R. J. W. Cysteine is the Initial Site of Modification of Alpha-Crystallin by Kynurenine. *Biochem. Biophys. Res. Commun.* **2000**, *276*, 216–223.

(20) Sherin, P. S.; Tsentalovich, Yu.P.; Snytnikova, O. A.; Sagdeev, R. Z. Photoactivity of Kynurenine-Derived UV-filters. *J. Photochem. Photobiol., B* **2008**, *93*, 127–132.

(21) Parker, N. R.; Jamie, J. F.; Davies, M. J.; Truscott, R. J. W. Protein-Bound Kynurenine is a Photosensitiser of Oxidative Damage. *Free Radical Biol. Med.* **2004**, *37*, 1479–1489.

(22) Mizdrak, J.; Hains, P. G.; Truscott, R. J. W.; Jamie, J. F.; Davies, M. J. Tryptophan-derived Ultraviolet Filter Compounds Covalently Bound to Lens Proteins are Photosensitizers of Oxidative Damage. *Free Radical Biol. Med.* **2008**, *44*, 1108–1119.

(23) Sherin, P. S.; Grilj, J.; Tsentalovich, Yu.P.; Vauthey, E. Ultrafast Excited-State Dynamics of Kynurenine - a UV Filter of the Human Eye. *J. Phys. Chem. B* **2009**, *113*, 4953–4962.

(24) Snytnikova, O. A.; Sherin, P. S.; Kopylova, L. V.; Tsentalovich, Yu.P. Kinetics and Mechanism of Reactions of Photoexcited Kynurenine with Molecules of Some Natural Compounds. *Rus. Chem. Bull.* **2007**, *56*, 732–738.

(25) Aquilina, J. A.; Truscott, R. J. W. Identifying Sites of Attachment of UV Filters to Proteins in Older Human Lenses. *Biochim. Biophys. Acta* **2002**, *1596*, 6–15.

(26) Eaton, D. F. Reference Materials for Fluorescence Measurement. *J. Photochem. Photobiol., B* **1988**, *2*, 523–531.

(27) Morandeira, A.; Engeli, L.; Vauthey, E. Ultrafast Charge Recombination of Photogenerated Ion Pairs to an Electronic Excited State. *J. Phys. Chem. A* **2002**, *106*, 4833–4837.

(28) Fürstenberg, A.; Julliard, M. D.; Deligeorgiev, T. G.; Gadjev, N. I.; Vasilev, A. A.; Vauthey, E. Ultrafast Excited-State Dynamics of DNA Fluorescent Intercalators: New Insight Into the Fluorescence Enhancement Mechanism. *J. Am. Chem. Soc.* **2006**, *128*, 7661–7669.

(29) Duvanel, G.; Banerji, N.; Vauthey, E. Excited-State Dynamics of Donor-Acceptor Bridged Systems Containing a Boron-Dipyrromethene Chromophore: Interplay Between Charge Separation and Reorientational Motion. *J. Phys. Chem. A* **2005**, *111*, 5361–5369.

(30) Molokov, I. F.; Tsentalovich, Yu.P.; Yurkovskaya, A. V.; Sagdeev, R. Z. Investigation of the Photo-Fries Rearrangement Reactions of 1- and 2-Naphthyl Acetates. *J. Photochem. Photobiol., A* **1997**, *110*, 159–165.

(31) Tsentalovich, Yu.P.; Kulik, L. V.; Gritsan, N. P.; Yurkovskaya, A. V. Solvent Effect on the Rate of β-Scission of the Tert-butoxyl Radical. *J. Phys. Chem. A* **1998**, *102*, 7975–7980.

(32) Bradford, M. M. A Rapid and Sensitive Method for the Quantitation of Microgram Quantities of Protein Utilizing the Principle of Protein-Dye Binding. *Anal. Biochem.* **1976**, *72*, 248–254.

(33) Lang, B.; Angulo, G.; Vauthey, E. Ultrafast Solvation Dynamics of Coumarin 153 in Imidazolium-Based Ionic Liquids. *J. Phys. Chem. A* **2006**, *110*, 7028–7034.

(34) Fürstenberg, A.; Vauthey, E. Ultrafast Excited-State Dynamics of Oxazole Yellow DNA Intercalators. *J. Phys. Chem. B* **2007**, *111*, 12610–12620.

(35) Taft, R. W.; Kamlet, M. J. The Solvatochromic Comparison Method. 2. The α-scale of Hydrogen-Bond Donor (HBD) Acidities. *J. Am. Chem. Soc.* **1976**, *98*, 2886–2894.

(36) Kamlet, M. J.; Abboud, J-L.M.; Abraham, M. H.; Taft, R. W. Linear Solvation Relationships. 23. A Comprehensive Collection of the Solvatochromic Parameters, π^*,α and β, and Some Methods for Simplifying the Generalized Solvatochromic Equation. *J. Org. Chem.* **1983**, *48*, 2877–2887.

(37) Snytnikova, O. A.; Sherin, P. S.; Tsentalovich, Yu. P. Biphotonic Ionization of Kynurenine and 3-Hydroxykynurenine. *J. Photochem. Photobiol., A* **2007**, *186*, 364–368.

(38) Bent, D. V.; Hayon, E. Excited State Chemistry of Aromatic Amino Acids and Related Peptides. III. Tryptophan. *J. Am. Chem. Soc.* **1975**, *97*, 2612–2619.

(39) Bryant, F. D.; Santus, R.; Grossweiner, L. I. Laser Flash Photolysis of Aqueous Tryptophan. *J. Phys. Chem.* **1975**, *79*, 2711–2716.

(40) Volkert, W. A.; Kuntz, R. R.; Ghiron, C. A.; Evans, R. F. Flash Photolysis of Tryptophan and N-acetyl-L-tryptophanamide; the Effect of Bromide on Transient Yields. *Photochem. Photobiol.* **1977**, *26*, 3–9.

(41) Posener, M. L.; Adams, G. E.; Wardman, P.; Cundall, R. B. Mechanism of Tryptophan Oxidation by Some Inorganic Radical-Anions: a Pulse Radiolysis Study. *J. Chem. Soc., Faraday Trans. 2* **1976**, *72*, 2231–2239.

(42) Feitelson, J.; Hayon, E. Electron Ejection and Electron Capture by Phenolic Compounds. *J. Phys. Chem.* **1973**, *77*, 10–15.

(43) Bent, D. V.; Hayon, E. Excited State Chemistry of Aromatic Amino Acids and Related Peptides. I. Tyrosine. *J. Am. Chem. Soc.* **1975**, *97*, 2599–2606.

(44) Sherin, P. S.; Gritsan, N. P.; Tsentalovich, Yu. P. Experimental and Quantum Chemical Study of Photochemical Properties of 4-Hydroxyquinoline. *Photochem. Photobiol. Sci.* **2009**, *8*, 1550–1557.

(45) Jarzeba, W.; Walker, G. C.; Johnson, A. E.; Kahlow, M. A.; Barbara, P. F. Femtosecond Microscopic Solvation Dynamics of Aqueous Solutions. *J. Phys. Chem.* **1988**, *92*, 7039–7041.

(46) Jimenez, R.; Fleming, G. R.; Kumar, P. V.; Maroncelli, M. Femtosecond Solvation Dynamics of Water. *Nature* **1994**, *369*, 471–473.

(47) Horng, M. L.; Gardecki, J. A.; Papazyan, A.; Maroncelli, M. Subpicosecond Measurements of Polar Solvation Dynamics: Coumarin 153 Revisited. *J. Phys. Chem.* **1995**, *99*, 17311–17337.

(48) Vaney, M. C.; Maignan, S.; Riès-Kautt, M.; Ducruix, A. High-Resolution Structure (1.33 Å) of a HEW Lysozyme Tetragonal Crystal Grown in the APCF Apparatus. Data and Structural Comparison with a Crystal Grown Under Microgravity from SpaceHab-01 Mission. *Acta Crystallogr.* **1996**, *D52*, 505–517.

JP104485K